2009

Opto-VLSI-based photonic true-time delay architecture for broadband adaptive nulling in phased array antennas

Budi Juswardy
Edith Cowan University

Feng Xiao
Edith Cowan University

Kamal Alameh
Edith Cowan University

Opto-VLSI-based photonic true-time delay architecture for broadband adaptive nulling in phased array antennas

Budi Juswardy, Feng Xiao, and Kamal Alameh

Centre for MicroPhotonic Systems, Edith Cowan University, Joondalup, WA, 6027, Australia
budij@ecu.edu.au, f.xiao@ecu.edu.au, k.alameh@ecu.edu.au

Abstract: This paper proposes a novel Opto-VLSI-based tunable true-time delay generation unit for adaptively steering the nulls of microwave phased array antennas. Arbitrary single or multiple true-time delays can simultaneously be synthesized for each antenna element by slicing an RF-modulated broadband optical source and routing specific sliced wavebands through an Opto-VLSI processor to a high-dispersion fiber. Experimental results are presented, which demonstrate the principle of the true-time delay unit through the generation of 5 arbitrary true-time delays of up to 2.5 ns each.

OCIS codes: (060.2310) Fourier optics; (070.1170) Fourier optics and signal processing; (060.2340) Fiber optics components; (350.4010) Microwaves.

References and links

1. J. Capmany, B. Ortega, D. Pastor, and S. Sales, "Discrete-time optical processing of microwave signals," J. Lightwave Technol. **23**, 702-723 (2005).
2. I. Frigyes and A. J. Seeds, "Optical generated true-time delay in phased array antennas," IEEE Trans. Microwave Theory Tech. **43**, 2378–2386 (1995).
3. V. Italia, M. Pisco, S. Campopiano, A. Cusano, and A. Cutolo, "Chirped Fiber Bragg Gratings for Electrically Tunable Time Delay Lines," IEEE J. Sel. Top. Quantum Electron. **11,** 408-416 (2005).
4. Y. Chen and R. T. Chen, "A fully packaged true time delay module for a K-band phased array antenna system demonstration," IEEE Photon. Technol. Lett. **14**, 1175–1177 (2002).
5. H. R. Rideout, J. S. Seregelyi, and J. Yao, "A True Time Delay Beamforming System Incorporating a Wavelength Tunable Optical Phase-Lock Loop," J. Lightw. Technol. **25,** 1961-1770 (2007).
6. R. Mital, C. M. Warnky, and B. L. Anderson, "Design and Demonstration of an Optical True-Time-Delay Device Based on an Octic-Style White Cell," J. Lightwave Technol. **24,** 982-990 (2006).
7. B. L. Anderson, D. J. Rabb, C. M. Warnky, and F. Abou-Galala, "Binary Optical True-Time Delay Based on the White Cell: Design and Demonstration," J. Lightwave Technol. **24**, 1886-1895 (2006).
8. B. L. Anderson and C. D. Liddle, "Optical true time delay for phased-array antennas: demonstration of a quadratic White cell," Appl. Opt. **41**, 4912-4921 (2002).
9. J. Shin, B. Lee, and B. Kim, "Optical True Time-Delay Feeder for X-Band Phased Array Antennas Composed of 2x2 Optical MEMS Switches and Fiber Delay Lines." IEEE Photon. Technol. Lett. **16**, 1364–1366 (2004).
10. G. Flamand, K. De Mesel, I. Moerman, B. Dhoedt, W. Hunziker, A. Kalmar, R. Baets, P. Van Daele, and W. Leeb, "InP-Based PIC for an Optical Phased-Array Antenna at 1.06μm," IEEE Photon. Technol. Lett. **12**, 876–878 (2000).
11. D. T. K. Tong and M. C. Wu, "Multiwavelength Optically Controlled Phased-Array Antennas," IEEE Trans. Microwave Theory Tech. **46**, 108–115 (1998).
12. Y. Jiang, B. Howley, Z. Shi, Q. Zhou, R. T. Chen, M. Y. Chen, G. Brost, and C. Lee, "Dispersion-Enhanced Photonic Crystal Fiber Array for a True Time Delay Structured X-Band Phased Array Antenna," IEEE Photon. Technol. Lett. **17**, 187–189 (2005).
13. O. Raz, R. Rotman, Y. Danziger, and M. Tur, "Implementation of Photonic True Time Delay using High-Order-Mode Dispersion Compensating Fibers," IEEE Photon. Technol. Lett. **16**, 1367–1369 (2004).
14. H. Zmuda, E. N. Toughlian, M. A. Jones, and P. M. Payson, "Photonic Architecture for Broadband Adaptive Nulling with Linear and Conformal Phased Array Antennas," Fiber Integr. Opt. **19**, 137-154 (2000).
15. H. Zmuda, E. N. Toughlian, and P. M. Payson, "Broadband Nulling for Conformal Phased Array Antennas Using Photonic Processing," IEEE Int. Top. Meeting Microwave Photon. MWP 2000, 17-19 (2000).

#103503 - $15.00 USD Received 31 Oct 2008; revised 4 Mar 2009; accepted 5 Mar 2009; published 11 Mar 2009

16. H. Zmuda, E. N. Toughlian, P. Payson, and H. W. Klumpe, "A Photonic Implementation of a Wide-Band Nulling System for phased Arays," IEEE Photon. Technol. Lett. **10**, 725-727 (1998).
17. F. Xiao, B. Juswardy, K. Alameh, and Y. T. Lee, "Novel broadband reconfigurable optical add-drop multiplexer employing custom fiber arrays and Opto-VLSI processors," Opt. Express **16**, 11703-11708 (2008).
18. I. G. Manolis, T. D. Wilkinson, M. M. Redmond, and W. A. Crossland, "Reconfigurable multilevel phase holograms for Optical switches," IEEE Photon. Technol. Lett. **14**, 801–803 (2002).
19. J. Capmany, B. Ortega, and D. Pastor, "A tutorial on Microwave photonic filters," J. Lightwave Technol. **24,** 201-229 (2006).
20. J. D. Taylor, L. R. Chen, and X. J. Gu, "Simple reconfigurable photonic microwave filter using an arrayed waveguide grating and fiber Bragg gratings," IEEE Photon. Technol. Lett. **19,** 510-512 (2007).
21. D. Pastor, B. Ortega, J. Capmany, S. Sales, A. Martinez, and P. Munoz, "Optical microwave filter based on spectral slicing by use of arrayed waveguide gratings," Opt. Lett. **28,** 1802-1804 (2003).

1. Introduction

The processing of radio frequency (RF) and microwave signals in the optical domain is an attractive approach to overcome the bottlenecks of bandwidth, power losses, and electromagnetic interference (EMI) encountered in conventional electronic signal processing systems [1]. A wide range of emerging RF signal processing applications require specifically high resolution, wide-range tunability, and fast reconfigurability. These requirements are difficult to achieve using conventional all-electronic processing, but feasible with photonics-based signal processing.

The use of photonics-based true time delay units to realise adaptive broadband phased-array antenna (PAA) beamformers has extensively been investigated in the last decade for applications ranging from modern microwave radar to wireless communication systems. In particular, broadband microwave phased-array antennas require the generation of variable true-time delays at each antenna element to realize beam or null steering, and optical fibers have been the best candidates for true-time delay synthesis. Compared with all-electrical techniques, optical true-time delay generation offers the advantages of broader bandwidth, lower insertion loss, higher phase stability, smaller size, lighter weight, and excellent immunity to both electromagnetic interference and crosstalk [2-5]. Several approaches have been adopted to realise tunable true-time delay units, including the use of in-fiber chirped Bragg gratings (FBGs) [3], white cells or fiber delay lines in conjunction with MEMS [6-9], integrated optical waveguides [10], optically-switched fiber delay structures [11], dispersion-enhanced photonic-crystal fibers [12], and higher-order mode dispersive multi-mode fibers [13]. However, while these reported true-time delay architectures have been efficient for realising beam steering in phased array antennas, they do not have the flexibility to simultaneously generate multiple arbitrary true-time delays, and this makes them impractical for broadband null steering [14]. Zmuda et al. have reported a few adaptive true-time delay architectures based on the use of multiple tunable lasers in conjunction with high-dispersion fibres for the implementation of broadband nulling in microwave phased arrays [14-16]. However, the use of multiple tunable lasers requiring continuous calibration makes the system implementation very expensive and impractical.

In this paper, we propose and demonstrate the principle of a novel true-time delay unit that employs an Opto-VLSI processor, a broadband optical source using Amplified Spontaneous Emission (ASE)**,** and high dispersion fibers that can be reconfigured to synthesize multiple arbitrary time delays. This true-time delay unit also has the capability to generate multiple true-time delays for several antenna elements simultaneously, making it attractive for broadband null-steering in phased array antennas.

2. Opto-VLSI processor

An Opto-VLSI processor is an array of liquid crystal (LC) cells driven by a Very-Large-Scale-Integrated (VLSI) circuit [17], as shown in Fig. 1(a). It is driven by digital holographic diffraction gratings capable of steering/shaping incident optical beams as illustrated in Fig. 1(b). The voltage level of each pixel can individually be controlled by using a few memory elements that select a discrete voltage level and apply it, through the aluminium mirror

#103503 - $15.00 USD Received 31 Oct 2008; revised 4 Mar 2009; accepted 5 Mar 2009; published 11 Mar 2009

electrode, across the LC cell. A transparent Indium-Tin Oxide (ITO) layer is used as the second electrode, and a quarter-wave-plate (QWP) layer is deposited between the LC and the aluminum mirror to accomplish polarization-insensitive operation [18].

By driving the Opto-VLSI with blazed gratings of different pitches, as shown in Fig. 1(b), optical beam steering can be achieved. The diffraction (or steering) angle for an Opto-VLSI processor, α_m, is given by [17]:

$$\alpha_m = \arcsin\left(\frac{m\lambda}{d}\right) \tag{1}$$

where m is the diffraction order (usually only the first order is considered), λ is the light wavelength in vacuum, and d is the grating period. By addressing each pixel independently a phase hologram can be synthesized leading to optical beam steering, beam shaping or multicasting.

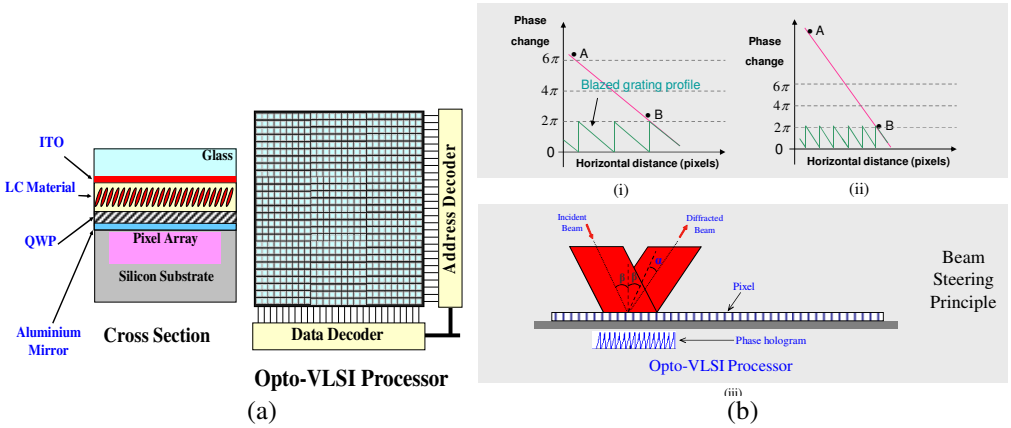

Fig. 1. (a) Opto-VLSI Processor layout and cell structure. (b) Principle of beam steering through variable-pitch blazed grating generation.

3. Phased-array antenna architecture for broadband null steering

Figure 2(a) shows a typical N-element phased-array antenna architecture, whose array factor (or directional response) is given by [16]:

$$AF_N(\theta) = \prod_{n=1}^{N-1}(x - x_n) = \sum_{m=0}^{N-1} W_m x^m \tag{2}$$

where $x = \exp\left[jkd\sin(\theta)\right]$, d is the antenna element spacing, k = wave number = ω/c, and $x_n = x(\theta_n)$ is a zero of the polynomial AF_N corresponding to an antenna null at the angular coordinate θ_n. Note that a change of even one zero affects all the weights, W_m. Note also that with N antenna elements, the phased-array antenna can synthesize only (N–1) nulls, as evident from Eq. (2).

Without loss of generality, considering a 4-element phased array antenna, with its main lobe at an angle θ and nulls located along angular coordinates, θ_1, θ_2, and θ_3, the array factor takes the form [14]:

$$AF_4(\theta) = \sum_{m=0}^{3} W_m e^{jmkd\sin(\theta)} = \left(e^{jkd\sin(\theta)} - e^{jkd\sin(\theta_1)}\right)\left(e^{jkd\sin(\theta)} - e^{jkd\sin(\theta_2)}\right)\left(e^{jkd\sin(\theta)} - e^{jkd\sin(\theta_3)}\right) \tag{3}$$

By expanding Eq. (3), we obtain

$$AF_4(\theta) = x^3 - x^2\left(e^{j\omega\tau_{21}} + e^{j\omega\tau_{22}} + e^{j\omega\tau_{23}}\right) + x\left(e^{j\omega\tau_{11}} + e^{j\omega\tau_{12}} + e^{j\omega\tau_{13}}\right) - e^{j\omega\tau_{01}} \tag{4}$$

From Eq. (4), it can be observed that for a 4-element phased array antennas, $2^{4-1}-1 = 7$ delay taps need to be generated by the true time delay unit in order to synthesis three nulls, and that the time delays required to be synthesized are:

#103503 - $15.00 USD Received 31 Oct 2008; revised 4 Mar 2009; accepted 5 Mar 2009; published 11 Mar 2009

$$\tau_{21} = \frac{d}{c}\sin(\theta_1), \tau_{22} = \frac{d}{c}\sin(\theta_2), \tau_{23} = \frac{d}{c}\sin(\theta_3)$$
$$\tau_{11} = \frac{d}{c}[\sin(\theta_1) + \sin(\theta_2)], \tau_{12} = \frac{d}{c}[\sin(\theta_1) + \sin(\theta_3)], \tau_{13} = \frac{d}{c}[\sin(\theta_2) + \sin(\theta_3)] \quad (5)$$
$$\tau_{01} = \frac{d}{c}[\sin(\theta_1) + \sin(\theta_2) + \sin(\theta_3)]$$

Generally, for an N-element broadband phased array, the synthesis of (N–1) broadband nulls can be achieved if the beamformer of the antenna can adaptively generate and combine $(2^{N-1} - 1)$ delayed versions of the RF signals received by the antenna elements, as illustrated in Fig. 2(b).

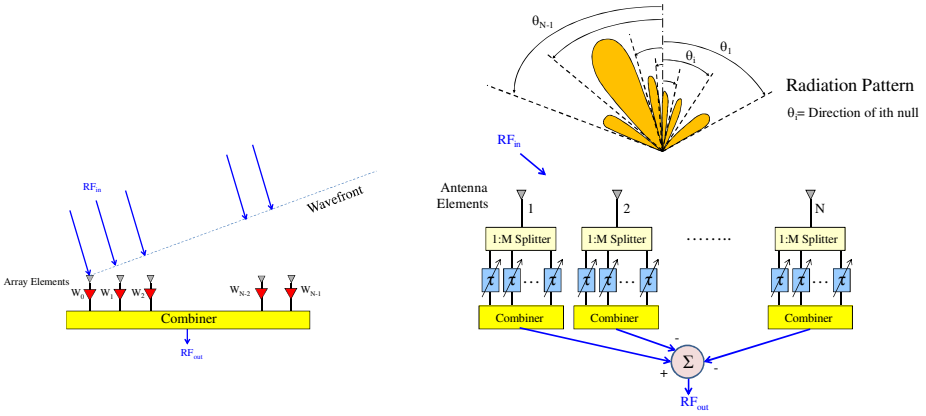

Fig. 2. (a) Typical phased-array antenna architecture. (b) Phased array antenna architecture for broadband null steering.

4. Proposed Opto-VLSI-based tunable true-time delay architecture for broadband null steering

Figure 3 shows the proposed Opto-VLSI-based microwave phased array antenna architecture for broadband null steering. It employs a broadband amplified spontaneous emission (ASE) source that is split into N parts, where N is the number of antenna elements. The RF signal received by an antenna element modulates the ASE signal through an Electro-optics Modulator (EOM) dedicated to that antenna element. Each RF-modulated optical signal is routed into an Erbium Doped Fiber Amplifier (EDFA) for amplification, and then collimated and launched into a diffractive grating plate. The latter demultiplexes the collimated ASE signal into wavebands (of different center wavelengths) along different directions and maps them onto the surface of a 2-D Opto-VLSI processor that is partitioned into N rectangular pixel blocks. Each pixel block is assigned to an antenna element and used to generate the delays required for that antenna element. Each pixel block is further partitioned into *M* rectangular sub-pixel-blocks, where each sub-pixel-block is assigned to an RF-modulated waveband.

By driving a sub-pixel-block with an appropriate phase hologram the RF-modulated waveband can be steered either along the incident path thus being coupled into its corresponding fiber collimator for maximum weight synthesis or off-track for arbitrary weight generation. The required voltage range for changing the phase of a pixel from 0 to 360 degrees is 5V. Therefore, single or multiple arbitrary RF-modulated wavebands can be coupled back into the various fiber collimators and the amplitude of each selected waveband can also be controlled simply by uploading the appropriate phase holograms that drive the various pixel-blocks of the Opto-VLSI processor.

#103503 - $15.00 USD Received 31 Oct 2008; revised 4 Mar 2009; accepted 5 Mar 2009; published 11 Mar 2009

The RF-modulated wavebands coupled into the fiber collimators are then routed via optical circulators to high dispersion optical fibers (HDFs), where they experience true-time delays that depend on their centre wavelengths. The delayed RF-modulated wavebands in the HDFs are finally detected by a photo-receiver array, and combined with appropriate polarities to synthesize the required nulls.

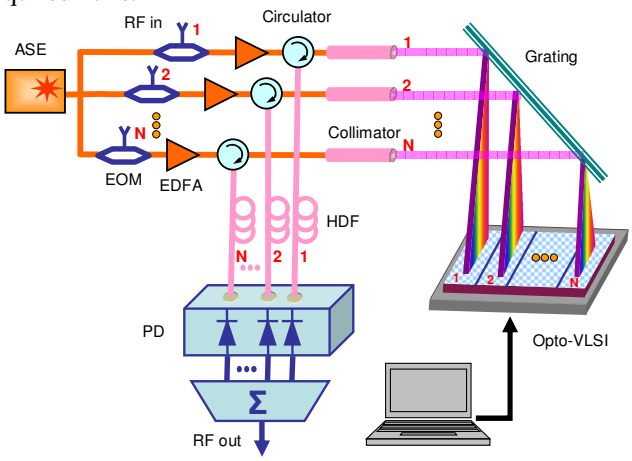

Fig. 3. Opto-VLSI-based phased array antenna architecture for broadband null steering.

One of the attractive features of the Opto-VLSI-based phased array antenna architecture shown in Fig. 3 is its ability to generate multiple RF delays without the need for RF splitters. Furthermore, the weight of each delayed RF sample can independently be controlled, adding flexibility to the beam and null steering capability of the antenna. This architecture offers excellent flexibility in null steering because multiple true-time RF delays for each antenna element can simultaneously be synthesized using computer generated holograms.

5. Experimental setup

The principle of the phased-array antenna architecture shown in Fig. 3 is demonstrated using the experimental setup illustrated in Fig. 4. In this setup, a broadband ASE source was modulated, via a JDS Uniphase electro-optical modulator (EOM) with a half-wave voltage of 6V, by an RF signal which was generated using a 20 GHz network analyzer. The RF-modulated optical signal was amplified by an EDFA and collimated at 1-mm diameter and then launched onto a diffractive grating plate. The latter demultiplexed the collimated ASE beam into multiple RF-modulated wavebands, which were then mapped onto the active window of a 256-phase-level 1×4096-pixel Opto-VLSI processor of 1-μm pixel size and 0.8-μm dead spacing between adjacent pixels.

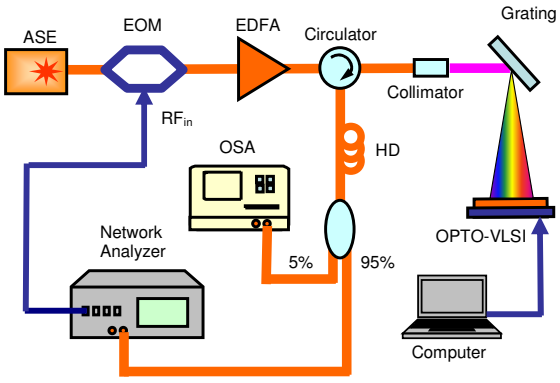

Fig. 4. Experimental setup used to demonstrate tunable time delay generation

#103503 - $15.00 USD Received 31 Oct 2008; revised 4 Mar 2009; accepted 5 Mar 2009; published 11 Mar 2009

Labview software was specially developed to generate optimised phase holograms that couple the specific RF-modulated wavebands back into the fiber collimator, and at the same time equalize their intensities by changing the maximum phase levels applied to the different pixel blocks [17]. For example, by applying an appropriate phase holograph consisting of 5 different blazed gratings, 5 different wavebands could be steered back and coupled to the collimator, as shown in Fig. 5. The selected wavebands were then routed via a circulator to a 22-km high dispersion fiber (HDF) of dispersion coefficient 382.5 ps/nm and insertion loss 4.6 dB. An optical spectrum analyzer (OSA) was used to monitor the spectrum detected by a photodiode built in the Network Analyzer, as illustrated in Fig. 4.

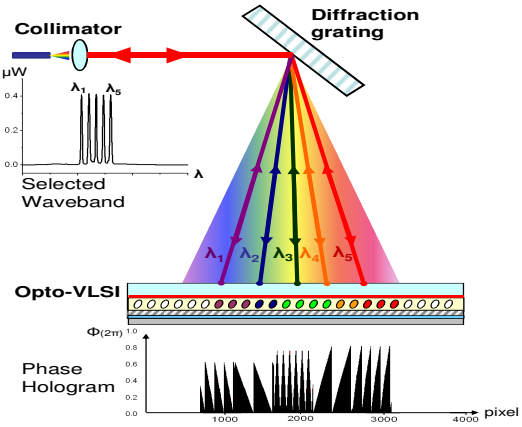

Fig. 5. The principle of optical waveband selection.

In order to measure the true-time delay between the wavebands, the network analyzer was set to measure the RF response produced after the photodetection of the delayed RF-modulated wavebands. The transfer function that results from detecting *M* wavebands can be described as [1]:

$$H(f) = \sum_{r=0}^{M} a_r \exp[-j2\pi r f \tau] \tag{6}$$

Where *f* is the RF frequency, *M* is the number of the detected RF-modulated wavebands, a_r is the r^{th} tap weight, which is proportional to the optical power of the r^{th} waveband, and τ is the time delay between adjacent wavebands introduced by the high dispersion fiber. The free spectral range of the transfer function is given by the following equation [1]:

$$f_{FSR} = \frac{1}{\tau} \tag{7}$$

The time delay, τ, can also be expressed in terms of the dispersion of the HDF as

$$\tau = \alpha \cdot \Delta\lambda \tag{8}$$

where α denotes the dispersion coefficient of the HDF, and $\Delta\lambda$ is the wavelength separation between the centers of two adjacent wavebands.

Note that, from Eq. (8), the time delay, τ, depends on the dispersion coefficient of the dispersion medium, therefore, a higher dispersion medium results in a longer maximum attainable time delay.

The RF insertion losses of the whole tunable true-time delay system, defined as the RF power ratio between input and output of the RF signal, can be approximately expressed as [19]:

#103503 - $15.00 USD Received 31 Oct 2008; revised 4 Mar 2009; accepted 5 Mar 2009; published 11 Mar 2009

$$T_{RF} = \frac{P_{RF\,out}}{P_{RF\,in}} = \left(\frac{\pi P_{opt} T_{opt} Z_0}{2V_\pi} R \right)^2 \tag{9}$$

Where Z_0 is the effective EOM RF input impedance or resistance of the EOM electrode, V_π is the voltage for a π-radian optical phase shift, R (A/W) is the photodetector responsivity, P_{opt} is the input continuous wave (CW) optical power to the EOM, and T_{opt} is the optical power transmission parameter that embraces all the optical losses and/or gain in the optical processing including the EOM insertion losses. In this experiment, the RF insertion loss is mainly due to the free-space optical system including the fibre collimator, the diffraction grating and the Opto-VLSI processor, which contributes around 12.5dB loss. Furthermore, the high dispersion fibre (HDF) and the EOM have insertion loss 4.6dB and 3.8dB, respectively. The total optical insertion loss of the entire system is around 21dB, whereas the EDFA provides a low gain of about 10dB due to saturation. The overall RF insertion loss in the experiment was about 25dB. However, this RF insertion loss can be compensated for by the use of an optical amplifier of 12.5dB gain placed after the HDF (before photodetection).

Different phase holograms, which are depicted in Fig. 6(a), were applied to the Opto-VLSI processor to generate five equally-separated RF-modulated optical wavebands with different wavelength separations as shown in Fig. 6(b). Fig. 6(c) shows the measured RF responses for seven true-time delay generation scenarios, corresponding to wavelength separations of 1.74nm, 2.64nm, 3.66nm, 4.32nm, 5.16nm, 5.88nm and 6.84nm, respectively.

The measured free spectral ranges of the various RF responses shown in Fig. 6(c) were used to calculate the true time delays, using Eq. (7). In addition, the measured waveband spacings (Fig. 6(b)) were also used to calculate the time delays for each scenario using Eq. (8). Table 1 summarizes the free spectral ranges of the various measured RF responses, the measured waveband separations, and their corresponding time delays calculated using Eq. (7) and Eq. (8), for the different scenarios. Excellent agreement between the true-time delays calculated using Eq. (7) and Eq. (8) is displayed in Table 1.

Note that the spectral response fades as the RF frequency increases, as shown in Fig. 6(c). This is due to the interaction between the dispersion of the HDF and the nonzero optical bandwidth of each waveband [20-21]. The bandwidth of the sliced wavebands in Fig. 6(b) was about 0.5nm, and this caused about 4dB spectral walk-off at 3GHz. This limits the practical bandwidth of the proposed true-time delay system. However if the sliced wavebands are narrow, the walk off effect becomes insignificant as reported in [21]. In addition, our preliminary experimental results have shown that a narrower waveband can be achieved using a higher dispersion grating plate and/or a larger distance between the grating and the Opto-VLSI processor.

#103503 - $15.00 USD Received 31 Oct 2008; revised 4 Mar 2009; accepted 5 Mar 2009; published 11 Mar 2009

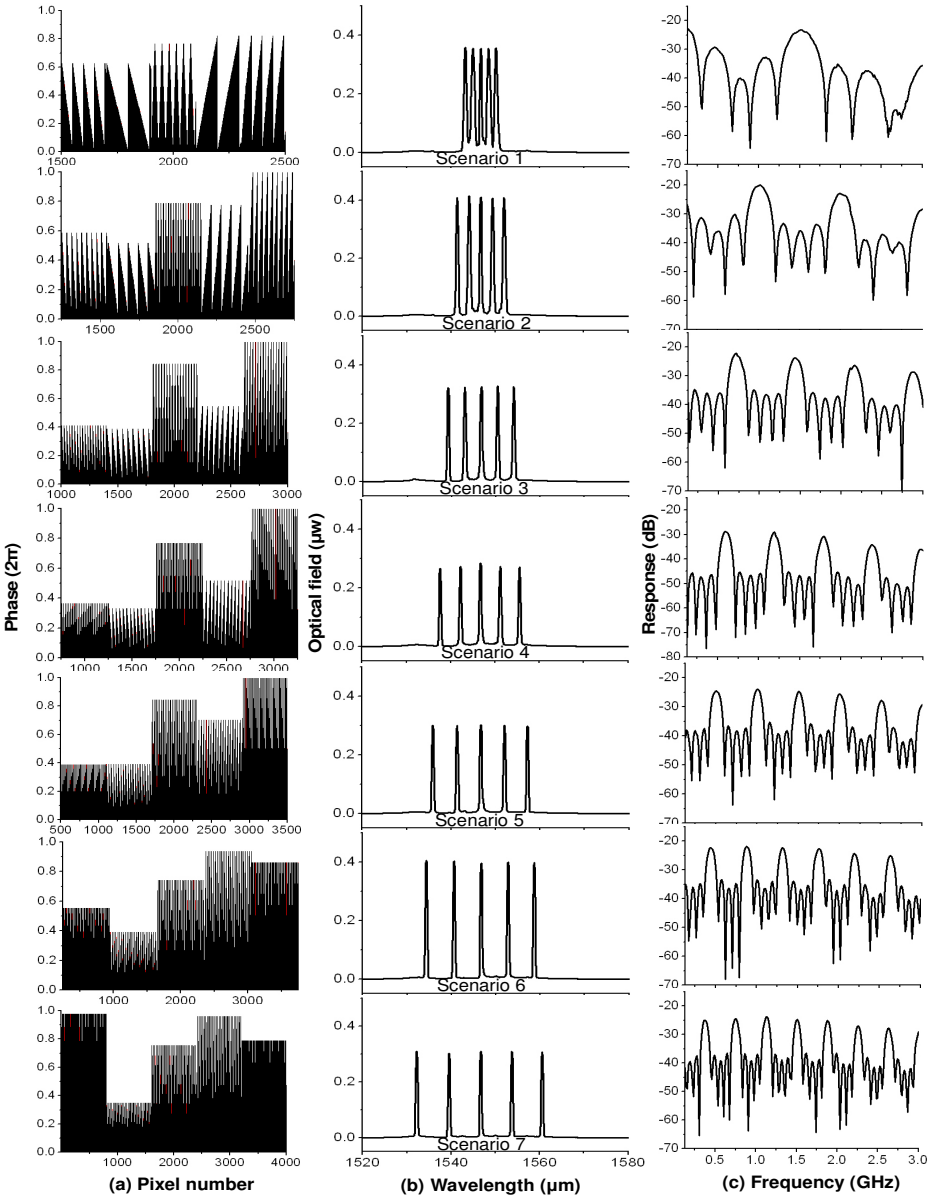

Fig 6: (a) Opto-VLSI hologram, (b) Optical spectrum of 5 RF-modulated wavebands, (c) Measured RF responses due to the photodetection of the RF-modulated wavebands displayed in (b).

Note that the number of multiple time delays that can be generated simultaneously depend on (i) the spectral width of the ASE source, (ii) the maximum delay time (i.e., the maximum wavebands separation), and (iii) the size of the active window of the Opto-VLSI processor. The larger the size of the active window of the Opto-VLSI processor, the larger the number of time delays that can be generated. On the other hand, the more wavebands are required (more nulls), the smaller the maximum waveband separation that could be achieved, thus limiting the null angle which can be synthesized. Note, however, that for a certain number of nulls, the required number of wavebands for each antenna element is fixed, as described in Eq. (2). In this case the ASE source should have sufficient spectral width to

#103503 - $15.00 USD Received 31 Oct 2008; revised 4 Mar 2009; accepted 5 Mar 2009; published 11 Mar 2009

ensure the synthesis of arbitrary null angles.

Finally, the experimental results shown in Fig. 6 and Table 1 confirm the ability of the Opto-VLSI-based true time delay unit to adaptively generate arbitrary RF delays for broadband null steering of phased array antennas. Note that, in order to realize a phased-array antenna beamformer that can synthesize broadband nulls, multiple RF true-time delays must be generated for each antenna element, as illustrated by Eq. (2). To achieve this, the Opto-VLSI processor was driven by optimised phase holograms that select and couple appropriate RF-modulated wavebands into an HDF that simultaneously delays the selected wavebands. To measure the generated time delays, the selected RF-modulated wavebands were detected by a single photodetector generating an RF transversal filter response. The FSR and shape factor of the RF filter response (measured by the network analyzer) were used in conjunction with Eqs. (7) and (8) to calculate the amplitudes and delay times of the wavebands.

Table. 1. Measured free spectral ranges, waveband separations, and their corresponding time delays calculated by Eq. 7 and Eq. 8.

	Scenario 1	**Scenario 2**	**Scenario 3**	**Scenario 4**	**Scenario 5**	**Scenario 6**	**Scenario 7**
Measured FSR (GHz)	1.51	0.98	0.72	0.60	0.50	0.43	0.39
Time delay (ns) calculated using Eq.7	**0.66**	**1.02**	**1.39**	**1.67**	**2.00**	**2.32**	**2.58**
Measured waveband separation (nm)	1.74	2.64	3.66	4.32	5.16	5.88	6.84
Time delay (ns) calculated using Eq.8	**0.67**	**1.02**	**1.41**	**1.66**	**1.99**	**2.26**	**2.63**

6. Conclusion

We have proposed and demonstrated the principle of an Opto-VLSI-based tunable true-time delay architecture for broadband null steering in phased-array antennas. Arbitrary single or multiple true-time delays have been synthesized by slicing an RF-modulated broadband optical source and routing arbitrary sliced wavebands through an Opto-VLSI processor to a high-dispersion fiber, where they experience RF delays that depend on their centre wavelengths. Experimental results have demonstrated the generation of 5 arbitrary true-time delays of up to 2.5 ns each. This true-time delay architecture is also attractive for a broad range of photonics-based RF signal processing applications.

#103503 - $15.00 USD Received 31 Oct 2008; revised 4 Mar 2009; accepted 5 Mar 2009; published 11 Mar 2009